Why hydrocarbon-cross-linked peptides are membrane permeable

Tzu-Lin Sun, Chang-Chun Lee, Yen Sun and Huey W. Huang*
Department of Physics & Astronomy, Rice University, Houston, Texas 77005, USA

*Corresponding: Huey W. Huang, hwhuang@rice.edu

Abstract

A new technology has been developed to overcome the delivery problem of peptide drugs. The technique utilizes a hydrocarbon linker ("staple") to stabilize a peptide in a helical configuration to promote cellular uptake. Here we investigate whether stapled peptides are intrinsically membrane permeable, by performing a case study on a stapled 12-mer peptide (an HIV-1 inhibitor CAI) named NYAD-1. We found that NYAD-1 indeed permeates through a lipid bilayer even at low solution concentrations. In order to understand the reason for the membrane permeability, we investigated the physical properties of peptide-lipid mixtures as a function of bound peptide-to-lipid molar ratio P/L. We found that NYAD-1 spontaneously binds to a lipid bilayer and subsequently exhibits three different states as P/L increases. At low P/L, the peptide primarily binds on the polar-apolar interface of the bilayer that has the effect of stretching the membrane area and thinning the membrane. The thinning effect reaches its maximum at P/L ~1/12. Further binding goes into the hydrocarbon region that has little thinning effect but continues to increase the membrane area. When the membrane area expanded 10-13%, transmembrane pores begin to appear in the bilayer. We believe that these membrane bound states explain the membrane permeability of NYAD-1at low peptide concentrations.

INTRODUCTION

The lipid matrix of a cell membrane provides a hydrophobic barrier that defines the boundary of the cell. An intact membrane is crucial for cell function but it is also a major impediment for the delivery of therapeutic agents into cells. This is so even if the drug enters the cell by endocytosis—in such a case, drug still needs to cross the endosomal membrane. In recent years a new type of drug technology called stapled peptides has been developed and adopted by the pharmaceutical industry. An all-hydrocarbon "staple" cross-links a peptide at i and i+4 or i+7 position to increase it's α-helix propensity (1-7). The rationale for the stapled peptides is three-fold (1): 1) stabilizing the peptide in a configuration that matches the binding site of the protein target, 2) protecting the peptide against proteolytic action and 3) making the peptide membrane permeable. While the functionality and stability of stapled peptides are understandable, it is not clear why the stapled helicity would facilitate cell uptake. Notably these stapled peptides bypass the Lipinski rules which stipulate that the molecular mass of a drug should not exceed 500 daltons (6, 8). Stapled peptides are several times that size, and yet still traffic to the intracellular targets (2, 4, 7). The goal of our study is to investigate first, if the peptides indeed gain membrane permeability by the stapling modification, and second, if so what could be the underlying mechanism for the membrane transmission property. We hope to provide a rational basis for the use of this new drug delivery technology. Understanding the mechanism for membrane transmission will facilitate the development of strategies for drug delivery.

We studied a stapled peptide called NYAD-1 based on a 12-mer peptide (CAI) that has been found to target the capsid of human immunodeficiency virus type 1 (HIV-1). CAI inhibits HIV-1 assembly *in vitro*; however it failed to inhibit HIV-1 in cell culture. The X-ray crystal structure of CAI in complex with the C-terminal domain of capsid (C-CA) revealed that the peptide adopts an α-helical conformation (4, 9). Accordingly Zhang et al. (4) used the hydrocarbon stapling technique (1-3) to convert CAI into a stable helical peptide named NYAD-1. Subsequently the authors showed the anti-HIV-1 activity of NYAD-1 in cell culture and that the stapled peptide indeed targeted the C-CA. However, cellular uptake is not a proof of self-permeating through the membrane. For example, cellular uptake of various cell penetrating peptides has been widely reported, yet the mechanisms of cell penetrating peptides are still being debated (10, 11).

With a fluorescence-labeled NYAD-1 (named NYAD-2) we found that the peptide indeed permeates across lipid bilayers. In order to understand what properties of the peptide enable the membrane permeability, we further studied the properties of NYAD-1mixed in lipid bilayers as a function of peptide-to-lipid ratio. The property of NYAD-1 in lipid bilayers is unlike other peptides or membrane-binding drugs we have studied before, including antimicrobial peptides, amyloidogenic peptides and amphipathic drugs. We offer a simple explanation for why a peptide gains membrane permeability by hydrocarbon stapling.

EXPERIMENT

Materials and sample preparation

NYAD-1 is H - Ile - Thr - Phe - X - Asp - Leu - Leu - X - Tyr - Tyr - Gly - Pro - NH_2 [with special cyclization to get double bond, X= (S) - alpha - (2'-pentenyl)alanine] (4). NYAD-1 and CAI (H-Ile-Thr-Phe-Glu-Asp-Leu-Leu-Asp-Tyr-Tyr-Gly-Pro-NH_2) were synthesized by CPC Scientific Inc (San Jose, CA) under the supervision of Xiaohe Tong, one of the authors of (4). NYAD-2 is FITC - (beta - Ala) - Ile - Thr - Phe - X - Asp - Leu - Leu - X - Tyr - Tyr - Gly - Pro - NH_2 (with special cyclization to get double bond, X= (S) - alpha - (2'- pentenyl)alanine; FITC = fluorescein isothiocyanate) synthesized by AnaSpec (Fremont, CA). 1,2-dioleoyl-sn-glycero-3-phosphocholine (DOPC) and 1,2-dioleoyl-sn-glycero-3-phosphoethanolamine-N-(lissamine rhodamine B sulfonyl) (Rh-DOPE) were purchased from Avanti Polar Lipids (Alabaster, AL). Texas red dextran (TRD) (MW 625 and 10000) and calcein (MW 623) were purchased from Invitrogen Probe (Grand Island, NY). Fluorescein PEG (MW 1000), was purchased from NANOCS (Boston, MA). All other chemicals were purchased from Sigma-Aldrich (St. Louis, MO) and were used without further purification. All experiments were performed at room temperature ~25^o C.

Giant unilamellar vesicles (GUVs) were produced by the electroformation method (12) in a production chamber containing a GUV interior solution. The solution includes ~200 mM sugar (sucrose or glucose) to control the osmolality and also a pH buffer and solution dyes if necessary. The osmolalities of the solutions used for GUV interior and GUV exterior were measured separately by a Wescor Model 5520 dew-point Osmometer (Wescor, Logan, UT). Equi-osmolality between the inside and outside of the GUV was the initial condition in all GUV experiments. To produce GUVs, DOPC or DOPC and 0.5% molar ratio of Rh-DOPE were dissolved in 1:1 (v/v) tetrafluoroethylene and chloroform. The lipid solution (~0.05 mg lipid) was deposited onto two ITO coated glass cover slips. After drying under vacuum, an o-ring was sandwiched between two ITO slips and the gap was filled with the interior solution. 3 V ac at 10 Hz was applied between the two ITO electrodes for 2 h. Subsequently the frequency was adjusted to 5 Hz for 10 mins and followed by 1 Hz for 10 mins. This electroformation method has been shown to produce unilamellar large vesicles (12). The GUV suspension was then gently collected in a glass vial (reservoir). The vesicles were used within 24 hrs of production.

Aligned multilamellae of peptide/lipid mixtures were prepared by first dissolving the peptide and lipid of chosen molar ratio, P/L, in 1:1 (v/v) tetrafluoroethylene and chloroform. The mixture was uniformly spread on a thoroughly cleaned fused-quartz substrate (0.018 mg peptide on a 1 cm^2 quartz plate for P/L>1/30; 0.3 mg of lipid on a 1 cm^2 plate for P/L≤1/30)**.** After the solvent evaporated in vacuum, the sample was hydrated with saturated water vapor in 37^o C oven overnight. The results were well-aligned parallel bilayers, as proven by x-ray diffraction. During the experiment, the samples were housed in a temperature humidity chamber in which the hydration level of the sample was controlled by the relative humidity (RH) of water vapor (13).

Aspirated GUV experiment

The experimental setup for aspirated GUV experiment was described in Sun et al (14). Before the experiment, micropipettes (with inner diameter 16-20 μm) and the walls of sample chambers were coated with 0.5% bovine serum albumin in order to dissipate the charge on the glass surface and then washed extensively with water. The micropipette was connected to an oil-filled U tube where a negative pressure was produced and controlled by reference to the atmosphere pressure (15).

A selected GUV (diameter ~40-70 μm) in the reservoir was aspirated at a low constant negative pressure (~100 Pa producing a membrane tension ~0.4 mN/m) by a micropipette, and transferred via a transfer pipe (14) to an observation chamber where the solution contained the peptide. Note that CAI, NYAD-1or NYAD-2 was added to the solution by first dissolving in DMSO. It is known that DMSO partially permeates through lipid bilayers (16). In order to avoid the effect of DMSO on osmolality balance (16), the same concentration of DMSO was also added to the interior solution, so that the osmolality of the solution in the observation chamber was the same as that of the GUV interior solution. The response of the GUV to the peptide binding was observed by a conventional inverted widefield microscope (IX81, Olympus, Tokyo, Japan) and recorded by a Hamamatsu Photonics digital CCD Camera (model C10600-10B) (Hamamatsu City, Japan), or a confocal microscopy (Nikon C1 si-LU4A confocal spectral imaging system and Nikon C2 confocal laser point scanning system—Tokyo, Japan) with 488nm/561nm lasers (OBIS/Sapphire, Coherent, Santa Clara, CA).

In response to peptide binding, a GUV can potentially change its membrane area A and volume V. The protrusion inside the micropipette serves as an amplifier for the measurement of such changes. From the microscopic images, L_p the length of the protrusion, R_p the radius of the micropipette, and R_v the radius of the GUV were carefully measured. Then it is straightforward to show $\Delta A = 2\pi R_p \Delta L_p + 8\pi R_v \Delta R_v$, and $\Delta V = \pi R_p^2 \Delta L_p + 4\pi R_v^2 \Delta R_v$ (17). In general the changes of GUV radius ΔR_v were too small to be measured accurately. However as long as the inside and outside of the GUVs were isotonic, there should be no change of volume. Under the condition $\Delta V = 0$, ΔL_p is directly proportional to ΔA: $\Delta A = 2\pi R_p\left(1 - R_p/R_v\right)\Delta L_p$. This is the case when the peptide binds to the GUV but does not cause any molecular leakage; the protrusion length increase $\Delta L_p > 0$ indicates an area expansion $\Delta A > 0$.

On the other hand, if peptides induce formation of finite-sized transmembrane pores, the influx of glucose will be greater than the efflux of sucrose through the pores, because sucrose is approximately two times as large as glucose. The resultant osmolality imbalance induces a net water influx, causing a volume increase in the GUV. If the membrane area is constant, the relation between ΔL_p and ΔV is $\Delta V = -\pi R_p\left(R_v - R_p\right)\Delta L_p$. Thus the GUV protrusion length would decrease, $\Delta L_p < 0$, when peptides induce pores in the membrane (18, 19).

To make a plot for aspirated GUV experiments, the protrusion length increase is converted to increasing $\Delta A/A$, using the relation $\Delta A = 2\pi R_p\left(1 - R_p/R_v\right)\Delta L_p$, so that different

size GUVs can be compared with each other. However when pores are formed, the decrease of L_p is not a decrease of A as explained above. Nevertheless, we still use the relation $\Delta A = 2\pi R_p\left(1 - R_p/R_v\right)\Delta L_p$ to show the decrease of L_p in the $\Delta A/A$ plot. Thus a decreasing $\Delta A/A$ is used to indicate pore formation in the $\Delta A/A$ plot, not a decrease in membrane area.

GUV Leakage experiment

For leakage experiment, the GUV interior solution also contained 30 μM calcein and 50 μM TRD10000. Two observation chambers containing the same solution 190 mM glucose and 10 mM HEPES pH 7 were set side by side. About 10 μL of the GUV suspension was injected into the first observation chamber and well-mixed with the solution in the chamber by stirring. About ten GUVs were transferred from the first to the second chamber via a transfer pipe. The purpose of this two-chamber procedure was to dilute the untrapped calcein and TRD in the solution external to the GUVs. In the second chamber, the GUVs settled at the bottom due to the density differential and were observed by a widefield microscope. The effect of peptide-induced leakage was observed by slowly injecting a small amount of isotonic solution containing NYAD-1 until the peptide concentration equal to 25 μM.

Membrane permeation experiment

We used FITC labeled NYAD (called NYAD-2) to observe membrane permeation. The fluorescence intensity of NYAD-2 depends on the pH value. This was a problem, because in general the GUV production by the electroformation method (12) is difficult in ionic solutions, for example in pH 7. Fortunately the production of GUVs in pH 9 was possible. Thus we investigated the permeation of NYAD-2 with a pH 7 solution outside and a pH 9 solution inside the GUV.

The interior solution for GUV production was 210 mM sucrose, 10 mM Tris buffer pH 9, 10μM TRD625 and 2.82mM DMSO. One control chamber and one observation chamber were used for the permeation experiment. Both chambers contained 210 mM glucose, 10 mM Tris buffer pH 7 and 2.82mM DMSO; only the observation chamber contained 2 μM NYAD-2. A GUV aspirated from the production chamber was first transferred to the control chamber to dilute the TRD in the exterior solution, and then transferred to the observation chamber for observation by the confocal microscope. The image was recorded in two channels 488 nm for FITC and 561 nm for TRD. The recording time was 0.5 s at 1 min interval to avoid excessive photobleaching.

X-ray diffraction experiment

Multilamellar samples were measured in a temperature-humidity chamber (13). ω-2θ diffraction was collected on a four-circle Huber goniometer (Huber Diffraktionstechnik, Rimsting, Germany), with a vertical line-focused Cu K_α source (λ=1.542 Å) operating at 35 kV and 15–30 mA. The incident beam was collimated by a horizontal soller slit and two vertical slits on the front and the back sides of the soller slit. The horizontal and vertical divergences of the

incident beam were 0.23^0 and 0.3^0, respectively. The diffracted beam first passed through a vertical slit and then was discriminated by a bent graphite monochromator (selected for 1.542 Å) before entering a scintillation detector. Thus the detector excluded Compton scattering, fluorescence and most of the X-rays from air scattering. This diffractometer was designed to minimize the background signal, thus allowing the measurement of high diffraction orders.

Before the measurement, the aligned multilayer sample was carefully positioned at the center of the X-ray beam and was oriented so that $\omega = 0^0$ and $\theta = 0^0$ coincided. We have established an elaborate routine for positioning and orienting the sample as described in Wu et al. (20). A two-dimensional ω-θ scan around the second or the third Bragg order was used to check the alignment of the ω-angle and the mosaic of the multilayers alignment. Typically the FWHM (full width half maximum) of the peak on the ω axis (of the ω- θ scan) was $0.2\text{-}0.3^0$ (example in (21)). Once the sample was properly positioned and aligned on the diffractometer, each ω-2θ scan was performed from $\omega=0.5^0$ to $\omega=7.5^0$ with a step size of $\Delta\omega=0.01^0$. An attenuator was used to prevent the first-order Bragg peak from saturating the detector. The scan was repeated 2–3 times at each of several hydration levels and averaged at each hydration level for data analysis. Measurements at several hydration levels were for the purpose of phase determination by the swelling method. Only the results of 98% RH are reported. (At RH above 98%, membrane samples tended to flow.)

The procedure of data reduction was described in many of our previous works (22, 23). Briefly, the measured diffraction intensity was first corrected for the attenuator absorption and for the detector's dead-time factor. After removing the background, data were corrected for sample absorption and diffraction volume. The integrated peak intensities were then corrected for the polarization and the Lorentz factors. The relative magnitude of the diffraction amplitude was the square-root of the integrated intensity. With their phases determined by the swelling method, the diffraction amplitudes were used to reconstruct the electron density profile of the bilayer. Across the bilayer profile, the phosphate peak to phosphate peak distance (PtP) was measured for the bilayer thickness. Measurements by the above described procedure have been done for various peptide-lipid mixtures for more than a decade, e.g., (20, 21, 23). We found in each case the measured PtP reproducible within ±0.2 Å.

RESULTS

(1) Aspirated GUV experiment

Fig. 1 shows separately the responses of a DOPC GUV to CAI, NYAD-1 and NYAD-2 all at the same concentration 8 μM at pH 7. There was no indication of CAI binding to the GUV over a long time (Fig. 1A). The very slow increase of the protrusion length was the same as in a control run with no peptide. The background increase (in the absence of peptides) was caused by a slow increase of osmolality in the exterior solution due to water evaporation. A higher osmolality in the exterior solution caused an efflux of water from the GUV. A decrease of GUV volume at constant membrane area caused an increase of the protrusion length. The experiment with CAI was repeated many times at different peptide concentrations (highest 40 μM) with the

same result, all similar to the background increase. The conclusion is that CAI does not bind to the lipid bilayers.

In the presence of 8 μM NYAD-1, the protrusion length immediately increased and reached a maximum within 15 s (Fig. 1B and 1D). This implies that during this time the peptide binding increased the bound ratio P/L, without causing molecular leakage. After reaching a maximum length, the protrusion length decreased indicating pores were formed in the membrane as explained in the experimental section. In this case, the background protrusion length increase was negligible in such a short time duration. From the maximum protrusion length increase, we calculate the maximum fractional area increase to be $\Delta A/A = 11 - 13\%$ (Fig. 1D). At lower NYAD-1 concentrations, e.g., 4 μM, the $\Delta A/A$ curves looked the same, also increased to $\Delta A/A = 10 - 15\%$ except that the time for reaching the maximum stretched to 60-100 s.

The same experiment was repeated for NYAD-2 to show that the FITC label on NYAD-1 did not alter the peptide's characteristic property (Fig. 1C and 1E). The modification by the FITC label considerably slowed the action of the peptide, indicating a lower binding coefficient to the bilayer (note the time scale). Nevertheless NYAD-2 also increased the protrusion length to a maximum and then caused its decrease, showing its pore forming capability. Because the experiment lasted for a long time compared with NYAD-1, a significant portion of the protrusion length increase was due to the osmolality increase in the exterior solution, caused by water evaporation as explained above.

(2) Leakage experiment

Fig. 2 demonstrates molecular leakage induced by NYAD-1 at high concentrations. A GUV containing green dye calcein (MW 623) and red dye TXD10000 (MW 10000) was in the observation chamber containing a solution of 190 mM glucose and 10 mM HEPES (pH 7). NYAD-1 in the same solution was slowly injected into the observation chamber until its final concentration was 25 μM. After a while (this time depended on the distance and speed of injection) both dyes were observed to leak out, while the GUV membrane remained intact. Understandably the leakage of calcein was faster than TRD10000 due to the difference in molecular weight. When the same leakage experiment was performed with antimicrobial peptide magainin, the pores at first allowed both large and small dye molecules to leak out but after a while only small molecules continued to leak out, implying pore size reduction with time (24). It is not clear from our leakage curves whether the large dye would leak out completely. It is clear that at high concentration, NYAD-1 induces pores in membranes. The pore size kinetics was not pursued, because it is probably of no interest to the therapeutic use of the drug at much lower concentrations.

(3) Membrane permeability experiment

First, we measured the fluorescence intensity of NYAD-2 at pH 9 and at pH 7, and found that the intensity at pH 9 was 1.7 times higher than at pH7. Second, we used an aspirated GUV in a solution containing 15 μM NYAD-2 to measure the relative binding coefficients at pH 7 and

pH 9 (Fig. 3C). Membrane binding was measured by the fractional area expansion $\Delta A/A$ of the GUV. The plateaued values of $\Delta A/A$ indicated that the binding coefficient of NYAD-2 to DOPC GUV at pH 7 is 2 to 3 times higher than at pH 9.

Because NYAD peptide forms pores at high concentrations, the permeation experiment was conducted at a low peptide concentration (2 μM) to avoid pore formation. Note that at 15 μM NYAD-2, the time for $\Delta A/A$ to plateau was ~ 2 min. We expected the permeation experiment to last much longer. To avoid photobleaching, we set the measurement interval 1 min for fluorescence intensity measurement. An aspirated GUV was imaged in the control chamber (where there was no NYAD-2) right before it was transferred to the observation chamber. It took ~ 1.5 min to readjust the confocal focus after the aspirated GUV was transferred to the observation chamber. Therefore the first point of observation was ~1.5 min after the GUV was exposed to 2 μM NYAD-2. The result is shown in Fig. 3. The protrusion length increased without any sign of decrease, indicating peptide binding without molecular leakage. The absence of molecular leakage was reconfirmed by the constant intensity of TRD625 inside the GUV. The fluorescent intensity of each dye was corrected by a background reading without the dye. The steady increase of the FITC fluorescence intensity inside the GUV indicates permeation of NYAD-2 through the GUV membrane.

For a null control experiment, the same permeability experiment was performed with fluorescein PEG (1000) replacing NYAD-2. As expected, no fluorescein PEG was detected inside the GUV.

(4) Membrane thinning by NYAD-1 binding

Electron density profiles obtained by X-ray diffraction show that the peptide-lipid mixtures formed well defined lipid bilayers (Fig. 4 A,B). The electron density of the peptides did not show up in the diffraction-based profiles, because the peptide positions were not correlated from bilayer to bilayer (diffraction is the result of electron density correlations (25)). However, whether the peptides were located on the polar-apolar interface or inserted in the hydrocarbon chain region, either condition was expected to increase the chain disorder. Indeed the central region of the profile was increasingly smoothed out as P/L increases (Fig. 4B). The most important effect of peptide binding is measured by the phosphate peak to phosphate peak distance across the bilayer (PtP). PtP is a measure of the bilayer thickness. It decreases more or less linearly with P/L up to ~ 1/12 and levels off for P/L >1/12 (Fig. 4C). This transition point (~1/12) is called the threshold value P/L*. Previous studies on antimicrobial peptides (AMPs) (26, 27) showed that AMPs caused a linear decrease of PtP with P/L and followed by a PtP leveling off, similar to NYAD-1. Neutron in-plane scattering showed that transmembrane pores were formed in the bilayers for P/L >P/L* but no pores were detected for P/L < P/L* (28-30). Thus for AMPs, P/L* is the threshold concentration for pore formation.

Membrane thinning and membrane area expansion are related due to the near incompressibility of the hydrocarbon volume in the chain region of lipid bilayer (31). The hydrocarbon volume is the membrane area A times the thickness of the hydrocarbon region *h*

which can be obtained from PtP by $h \approx PtP - 10$ Å, namely, *PtP* minus twice the length of the glycerol region (from the phosphate to the first methylene of the hydrocarbon chains) (32, 33). The incompressibility of lipid chain volume, $\Delta(A \cdot h) = 0$, leads to an equality between the fractional area expansion and the fractional membrane thinning: $\Delta A/A = -\Delta h/h$. For NYAD-1 at P/L* ~ 1/12, when the membrane thinning reaches the maximun (Fig. 4D), the fractional thinning is $(-\Delta h/h)_{max}$~8%. At the corresponding value of membrane expansion $\Delta A/A$~8% in the GUV experiment, no pores were formed (Fig. 1D). Thus NYAD-1 is distinctly different from AMPs, although it is capable of pore formation.

DISCUSSION

A method for measuring membrane permeation

It is commonly assumed that a membrane-binding amphipathic molecule would bind on the outer leaflet of the membrane bilayer and would not translocate across the membrane. This is undoubtedly the case if the molecule is a globular protein and only a portion of the protein binds to the outer leaflet. For small drugs, the Lipinski rules disfavor the membrane permeation of molecules larger than 500 daltons (6, 8). Thus the questions are for membrane active peptides of molecular weights from 1000 to 4000 daltons, such as AMPs, cell penetrating peptides and peptide drugs. Does each of them permeate across the membrane upon binding? The answers are directly related to their functions in the case of cell-penetrating peptides and drugs or to their mechanisms in the case of AMPs. For example, it has been argued that pore formation by AMPs is due to the stress of asymmetric binding to the outer leaflet (24). To our knowledge, few permeability experiments have been performed so far, probably because of the difficulty of detecting the peptides and also because a meaningful test must be conducted at biologically relevant concentrations which are usually low. In the case of pore forming peptides, the test must be performed without pore formation.

For the drug NYAD, we have shown that the FITC labeled NYAD-2 has the same characteristic property of NYAD-1 in membrane interactions. Two factors favor the permeation experiment with NYAD-2. First, we discovered that it was possible to produce GUVs in a pH 9 solution (although not in pH 7). A previous experiment by Zhou and Raphael (34) showed that there was little change of bilayer elastic properties between pH 7 and pH 9. The fluorescence intensity of NYAD-2 at pH 9 was measured to be 1.7 time higher than at pH 7. Thus if NYAD-2 does permeate into the interior of GUV, the fluorescence intensity would be enhanced for detection. Second, we found that the binding coefficient of NYAD-2 to DOPC GUV at pH 7 is 2 to 3 times higher than at pH 9 (Fig. 3C). That means that at a given surface bound concentration of NYAD-2 on the membrane, the equilibrium solution concentration of NYAD-2 at pH 9 is 2 to 3 times larger than the equilibrium solution concentration at pH 7. Thus, supposing that NYAD-2 is freely permeating across the membrane, the equilibrium NYAD-2 concentration at pH 9 inside the GUV would be 2 to 3 times higher than the equilibrium NYAD-2 concentration at pH 7 outside the GUV.

The permeation experiment (Fig. 3A, B) clearly shows that NYAD-2 peptides diffused from the outside solution into the GUV by permeating through the membrane, while the integrity of the membrane was assured by no decrease of the GUV protrusion length (see the experimental section on aspirated GUV) and no leakage of TRD625. As predicted, the accumulated NYAD-2 inside the GUV exceeded the outside concentration.

Membrane-bound states and membrane permeability

Although NYAD-1 induces pore formation at a very high peptide-to-lipid ratio in bilayers, its behavior is different from pore-forming peptides like melittin and other AMPs. NYAD-1 and AMPs all initially bind to the polar-apolar interface of bilayers, where they cause membrane area expansion in a GUV and membrane thinning in a lipid bilayer, in direct proportion to P/L. The maximum fractional membrane thinning $(-\Delta h/h)_{max}$ caused by AMPs is typically in the range of 3 to 5 %, right before the AMPs form pores (26). At the corresponding value of $\Delta A/A$, the GUV begins to leak or shows signs of pore formation (19). Thus the value of P/L when the maximum membrane thinning occurs is called the threshold concentration P/L* of AMPs for pore formation. For AMPs, $(-\Delta h/h)_{max} = (-\Delta A/A)_{max}$.

NYAD-1 is fundamentally different from AMPs. Firstly the maximum membrane thinning by NYAD-1 (~8%) exceeds the maximum thinning (~5%) by any AMP (26). An ~8% membrane thinning is probably the physical limit of lipid bilayers, because $\Delta A/A \sim 8\%$ is also the limit of lipid bilayer area expansion by external tension (35). Secondly when NYAD-1 binding caused the GUV area expansion to $\Delta A/A \sim 8\%$ there was no pore formation (Fig. 1D). As the binding of NYAD-1 continued, the GUV continued its membrane area expansion until $\Delta A/A = 11 - 13\%$ when pores appeared in the membrane. The simplest explanation is that NYAD-1 initially binds on the bilayer interface that causes both membrane area expansion and membrane thinning, $\Delta A/A = -\Delta h/h$ in direct proportion to P/L. But after the membrane thinning reaches the physical limit of $(-\Delta h/h)_{max}$ ~8%, further binding of NYAD-1 goes into the hydrocarbon region of the bilayer which further expands the membrane area by incorporating the peptides in the chain region without the effect of membrane thinning, $\Delta A/A = (-\Delta h/h)_{max} + (a\_p)/A$, where (a_p) is the area expansion due to NYAD-1 in the hydrocarbon region. Only when the area expansion reaches $\Delta A/A \sim 11 - 13\%$ the pores begin to appear in the membrane—at that point there is a significant concentration of peptides inserted in the lipid chain region.

The pore formation by NYAD-1 occurs at such high peptide to lipid ratios, it is probably irrelevant to the therapeutic use of NYAD-1. However it is the existence of bound states in the hydrocarbon region that makes NYAD-1 capable of translocating across the membrane. For the same reason AMPs are capable of translocating across membrane by forming transient pores that do not allow molecular leakage but allow passage of atomic ions. It is well known that transient single-channels by AMPs were detected in ion conduction experiments at peptide concentrations in the nanomolar range (36), much lower than the pore-forming threshold concentrations of AMPs which are in the micromolar range (36, 37).

Thus we understand the effect of a hydrocarbon-staple as follows. First, the hydrocarbon link provides an amphiphathic molecular surface to an otherwise hydrophilic peptide. CAI does not bind to lipid bilayers, but NYAD-1 does. Second, the cross-linking stabilizes the peptide in a helical form, that is also compatible with the chain region of lipid bilayers. This is not a trivial property because there are amphipathic molecules that spontaneously bind to the bilayer interface but do not insert into the chain region of lipid bilayers. Examples include tea catechin (14), penetratin (38) and islet amyloid polypeptide (IAP) (39). Both penetratin and IAP are random coils in solution and spontaneously bind to the bilayer interface as α-helices, but unlike NYAD-1, they do not insert into the hydrocarbon region. Experiments of penetratin and IAP showed that as each peptide concentration in the bilayer increased to a P/L*, both peptides turned into β-sheet-aggregates and exited from the bilayer (38, 39). Thus another possible function of the hydrocarbon stapling might be preventing the peptide from turning into β-sheet-aggregates.

ACKNOWLEDGMENTS

This work was supported by NIH (US) Grant GM55203 and by the Robert A. Welch Foundation Grant C-0991.

References

1. Schafmeister, C. E., J. Po, and G. L. Verdine. 2000. An All-Hydrocarbon Cross-Linking System for Enhancing the Helicity and Metabolic Stability of Peptides. Journal of the American Chemical Society 122:5891-5892.
2. Walensky, L. D., A. L. Kung, I. Escher, T. J. Malia, S. Barbuto, R. D. Wright, G. Wagner, G. L. Verdine, and S. J. Korsmeyer. 2004. Activation of apoptosis in vivo by a hydrocarbon-stapled BH3 helix. Science 305:1466-1470.
3. Bernal, F., A. F. Tyler, S. J. Korsmeyer, L. D. Walensky, and G. L. Verdine. 2007. Reactivation of the p53 tumor suppressor pathway by a stapled p53 peptide. J Am Chem Soc 129:2456-2457.
4. Zhang, H., Q. Zhao, S. Bhattacharya, A. A. Waheed, X. Tong, A. Hong, S. Heck, F. Curreli, M. Goger, D. Cowburn, E. O. Freed, and A. K. Debnath. 2008. A cell-penetrating helical peptide as a potential HIV-1 inhibitor. J Mol Biol 378:565-580.
5. Kutchukian, P. S., J. S. Yang, G. L. Verdine, and E. I. Shakhnovich. 2009. All-atom model for stabilization of alpha-helical structure in peptides by hydrocarbon staples. Journal of American Chemical Society 131:4622-4627.
6. Arora, P. S., and A. Z. Ansari. 2009. Chemical biology: A Notch above other inhibitors. Nature 462:171-173.
7. Moellering, R. E., M. Cornejo, T. N. Davis, C. Del Bianco, J. C. Aster, S. C. Blacklow, A. L. Kung, D. G. Gilliland, G. L. Verdine, and J. E. Bradner. 2009. Direct inhibition of the NOTCH transcription factor complex. Nature 462:182-188.
8. Lipinski, C. A., F. Lombardo, B. W. Dominy, and P. J. Feeney. 2001. Experimental and computational approaches to estimate solubility and permeability in drug discovery and development settings. Adv Drug Deliv Rev 46:3-26.
9. Ternois, F., J. Sticht, S. Duquerroy, H. G. Krausslich, and F. A. Rey. 2005. The HIV-1 capsid protein C-terminal domain in complex with a virus assembly inhibitor. Nat Struct Mol Biol 12:678-682.
10. Yang, S. T., E. Zaitseva, L. V. Chernomordik, and K. Melikov. 2010. Cell-penetrating peptide induces leaky fusion of liposomes containing late endosome-specific anionic lipid. Biophys. J. 99:2525-2533.
11. Madani, F., S. Lindberg, U. Langel, S. Futaki, and A. Graslund. 2011. Mechanisms of cellular uptake of cell-penetrating peptides. J Biophys 2011:414729.
12. Angelova, M. I. 2000. Liposome Electroformation. In Giant Vesicles. P. L. Luisi, and P. Walde, editors. John Wiley & Sons, Chichester. pp. 27-36.
13. Yang, L., and H. W. Huang. 2003. A rhombohedral phase of lipid containing a membrane fusion intermediate structure. Biophys J 84:1808-1817.
14. Sun, Y., W. C. Hung, F. Y. Chen, C. C. Lee, and H. W. Huang. 2009. Interaction of tea catechin (-)-epigallocatechin gallate with lipid bilayers. Biophys J 96:1026-1035.
15. Fygenson, D. K., M. Elbaum, B. Shraiman, and A. Libchaber. 1997. Microtubules and vesicles under controlled tension. Phys. Rev. E 55:850-859.
16. Sun, Y., C. C. Lee, W. C. Hung, F. Y. Chen, M. T. Lee, and H. W. Huang. 2008. The bound states of amphipathic drugs in lipid bilayers: study of curcumin. Biophys J 95:2318-2324.
17. Kwok, R., and E. Evans. 1981. Thermoelasticity of large lecithin bilayer vesicles. Biophys J 35:637-652.
18. Longo, M. L., A. J. Waring, L. M. Gordon, and D. A. Hammer. 1998. Area expansion and permeation of phospholipid membrane bilayer by influenza fusion peptides and melittin. Langmuir 14:2385-2395.
19. Lee, M. T., W. C. Hung, F. Y. Chen, and H. W. Huang. 2008. Mechanism and kinetics of pore formation in membranes by water-soluble amphipathic peptides. Proc Natl Acad Sci U S A 105:5087-5092.

20. Wu, Y., K. He, S. J. Ludtke, and H. W. Huang. 1995. X-ray Diffraction Study of Lipid Bilayer Membrane Interacting with Amphiphilic Helical Peptides: Diphytanoyl Phosphatidylcholine with Alamethicin at Low Concentrations. Biophys J 68:2361-2369.
21. Weiss, T. M., P. C. van der Wel, J. A. Killian, R. E. Koeppe, 2nd, and H. W. Huang. 2003. Hydrophobic mismatch between helices and lipid bilayers. Biophys J 84:379-385.
22. Olah, G. A., H. W. Huang, W. H. Liu, and Y. L. Wu. 1991. Location of ion-binding sites in the gramicidin channel by X-ray diffraction. J Mol Biol 218:847-858.
23. Harroun, T. A., W. T. Heller, T. M. Weiss, L. Yang, and H. W. Huang. 1999. Experimental evidence for hydrophobic matching and membrane-mediated interactions in lipid bilayers containing gramicidin. Biophys J 76:937-945.
24. Tamba, Y., H. Ariyama, V. Levadny, and M. Yamazaki. 2010. Kinetic pathway of antimicrobial peptide magainin2 induced pore formation in lipid membranes. J. Phys. Chem. B 114:12018-12026.
25. Warren, B. E. 1990. X-ray Diffraction. Dover Publications,, Mineola, N.Y.; pp. 41-47, 51-54.
26. Huang, H. W. 2006. Molecular mechanism of antimicrobial peptides: the origin of cooperativity. Biochim Biophys Acta 1758:1292-1302.
27. Lee, C. C., Y. Sun, S. Qian, and H. W. Huang. 2011. Transmembrane pores formed by human antimicrobial peptide LL-37. Biophys J 100:1688-1696.
28. He, K., S. J. Ludtke, D. L. Worcester, and H. W. Huang. 1996. Neutron scattering in the plane of membranes: structure of alamethicin pores. Biophys J 70:2659-2666.
29. Ludtke, S. J., K. He, W. T. Heller, T. A. Harroun, L. Yang, and H. W. Huang. 1996. Membrane pores induced by magainin. Biochemistry 35:13723-13728.
30. Yang, L., T. A. Harroun, T. M. Weiss, L. Ding, and H. W. Huang. 2001. Barrel-stave model or toroidal model? a case study on melittin pores. Biophys J 81:1475-1485.
31. Seemann, H., and R. Winter. 2003. Volumetric properties, compressibilities, and volume flucturations in phospholipid-cholesterol bilayers. Z. Phys. Chem. 217:831-846.
32. McIntosh, T. J., and S. A. Simon. 1986. Area per molecule and distribution of water in fully hydrated dilauroylphosphatidylethanolamine bilayers. Biochemistry 25:4948-4952.
33. Hung, W. C., F. Y. Chen, and H. W. Huang. 2000. Order-disorder transition in bilayers of diphytanoyl phosphatidylcholine. Biochim Biophys Acta 1467:198-206.
34. Zhou, Y., and R. M. Raphael. 2007. Solution pH alters mechanical and electrical properties of phosphatidylcholine membranes: relation between interfacial electrostatics, intramembrane potential, and bending elasticity. Biophys J 92:2451-2462.
35. Evans, E., V. Heinrich, F. Ludwig, and W. Rawicz. 2003. Dynamic tension spectroscopy and strength of biomembranes. Biophys J 85:2342-2350.
36. Merrifield, R. B., E. L. Merrifield, P. Juvvadi, D. Andreu, and H. G. Boman. 1994. Design and synthesis of antimicrobial peptides. In Antimicrobial Peptides. H. G. Boman, J. Marsh, and J. A. Goode, editors. John Wiley & Sons, Chichester. 5-26.
37. Zasloff, M. 2002. Antimicrobial peptides of multicellular organisms. Nature 415:389-395.
38. Lee, C. C., Y. Sun, and H. W. Huang. 2010. Membrane-mediated peptide conformation change from alpha-monomers to beta-aggregates. Biophys J 98:2236-2245.
39. Lee, C. C., Y. Sun, and H. W. Huang. 2012. How type II diabetes-related islet amyloid polypeptide damages lipid bilayers. Biophys J 102:1059-1068.

FIGRUE LEGENDS

Figure 1 An aspirated GUV of DOPC (and 0.5% molar ratio of Rh-DOPE) was exposed to a solution containing 8 μM CAI (A), 8 μM NYAD-1 (B) and 8 μM NYAD-2 (C) at pH 7. The osmolalities of the interior and exterior solutions were initially balanced. Slow water evaporation caused a slow increase of osmolality in the exterior solution resulting in a slow background increase of the protrusion length with time similar to (A), which was negligible within 5 mins. (A) CAI did not cause protrusion length increase beyond the background increase, indicating no binding to the bilayer. (B) and (C) NYAD-1 and NYAD-2 bound to the lipid bilayer and caused the protrusion length increase initially. After the protrusion length reached a maximum it gradually decreased indicating pore formation. Note the time scale differences in (B) and (C). The protrusion length change in (B) and (C) was converted to the fractional area change $\Delta A/A$ in (D) and (E), respectively. Scale bar = 25 μm.

Figure 2 A GUV (DOPC) containing green dye calcein (MW 623) and red dye TXD (MW 10000) was in an isotonic solution at pH 7. NYAD-1 was added slowly to the outside solution until it reached 25 μM. Both dyes started to leak out at the same time (time zero is an arbitrary reference point). Scale bar = 50 μm.

Figure 3 (A) Confocal images of an aspirated GUV (DOPC) containing 10μM TRD625 (red) exposed to 2 μM NYAD-2 (green). The first image was taken in the control chamber (without NYAD-2) right before the transfer to the observation chamber, time = 0. The fluorescent intensity of NYAD-2 inside the GUV was enhanced by the pH 9 effect (see text). The binding of NYAD-2 caused the membrane expansion with no molecular leakage (protrusion length increase). (The horizontal red bar on the micropipette was an optical artifact.) Scale bar = 50 μm. (B) Relative intensities of fluorescence: Red for TRD625 inside the GUV; Black for the background intensity of NYAD-2 outside the GUV; Green for the intensity of NYAD-2 inside the GUV normalized to the intensity outside (including the pH 9 effect). Note that the relative intensity inside exceeded the intensity outside after 10 mins (see the explanation in text). (C) The binding of 15 μM NYAD-2 to DOPC GUV at pH 7 and at pH 9, expressed in the fractional membrane area expansion $\Delta A/A$. The binding coefficient of NYAD-2 to DOPC at pH 7 is 2 to 3 times higher than at pH 9.

Figure 4 X-ray lamellar diffraction of NYAD-1 and DOPC mixtures at a series of P/L. (A) Raw data of the diffraction patterns. (B) Electron density profiles of the bilayers: Z is the distance from the bilayer center. (C) The phosphate peak to phosphate peak distance across the bilayer, PtP, measured for a series of P/L.

Figure 1

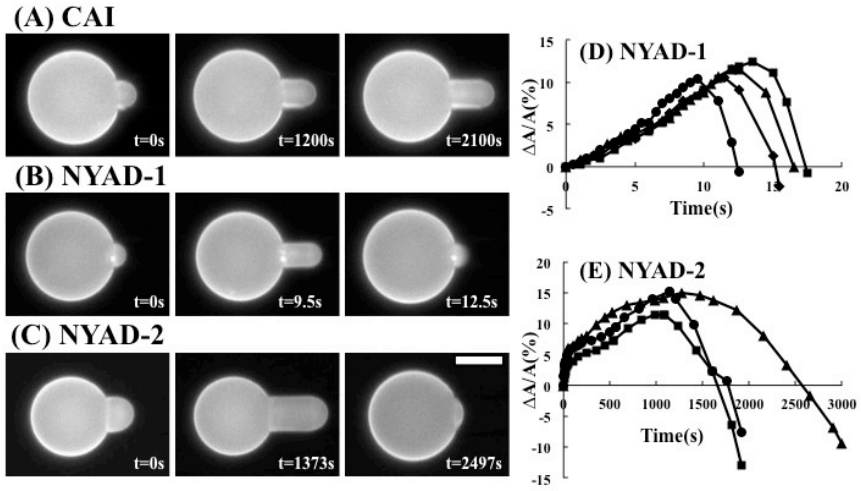

Figure 2

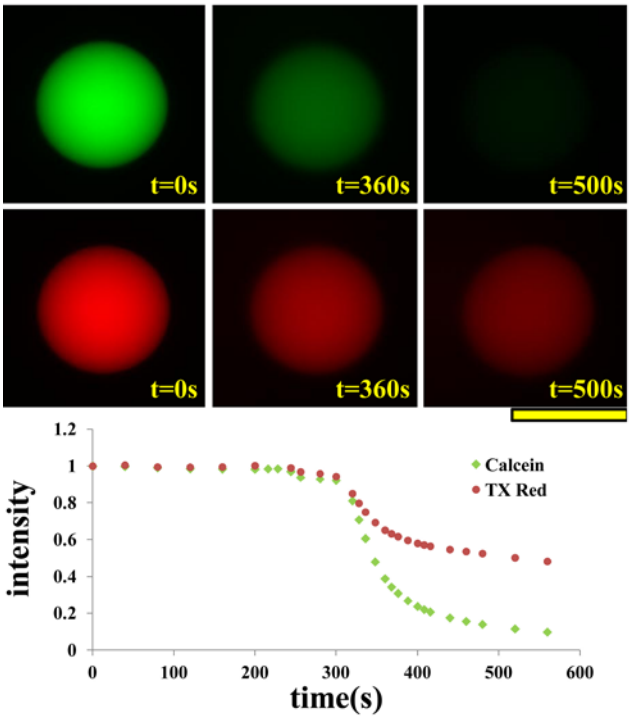

Figure 3

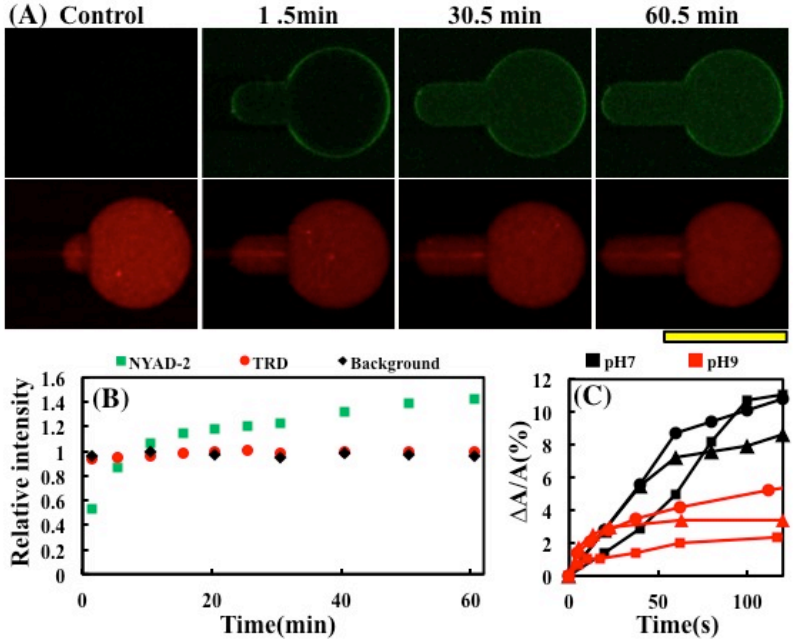

Figure 4